Available online at www.sciencedirect.com

SCIENCE DIRECT®

Coastal Engineering 52 (2005) 673–689

Coastal Engineering
An International Journal for Coastal, Harbour and Offshore Engineers

www.elsevier.com/locate/coastaleng

Bedload sediment transport in coastal waters

Richard L. Soulsby*, Jesper S. Damgaard[1]

HR Wallingford Ltd, Howbery Park, Wallingford, Oxon, OX10 6RX, UK

Received 30 June 2004; received in revised form 14 February 2005; accepted 20 April 2005
Available online 17 June 2005

Abstract

Formulae for bedload transport of sediments in conditions characteristic of coastal waters are developed from principles of physics. They cover driving forces of: current alone, current plus symmetrical waves, current plus asymmetrical waves, asymmetrical waves alone, and integrated longshore transport. In each case the transport is given as one or more analytical functions of the basic input variables. The formulae are tested against laboratory and field data, and give predictions that lie within a factor of 2 of the measured values for between 47% and 91% of the data, depending on the driving force. The formulae are suited to practical application in coastal waters, especially for transport of coarse materials such as shingle, and also for the bedload component of transport of sand.

Keywords: Sediment transport; Bedload; Coastal processes; Shingle; Longshore transport

1. Introduction

The movement of coarse sediments, such as shingle, in coastal waters takes place predominantly as bedload transport. For gravel grains coarser than 2 mm the transport can be considered to consist entirely of bedload motion. For coarse sands (say coarser than 0.3 mm) a large proportion will move as bedload, supplemented by suspension in the more extreme wave and current conditions. Even for sands finer than 0.3 mm, for which suspension may be the dominant transport mode, bedload transport cannot be neglected. It is possible that the evolution of bed morphology at a local scale may depend more strongly on bedload than suspension, because bedload reacts quickly to local flow conditions, whereas suspended sediment does not. We here derive and test formulae for predicting bedload transport in coastal waters.

The forcing conditions in coastal waters will usually comprise a combination of waves and currents. The waves will produce asymmetric bottom orbital velocities in shallow water, stronger and in the direction of wave propagation under the crests and weaker (but of longer duration) and against the direction of wave propagation under the troughs. We derive formulae in turn for the cases of current alone, current

* Corresponding author. Fax: +44 1491 825 916.
E-mail addresses: r.soulsby@hrwallingford.co.uk (R.L. Soulsby), j.damgaard@hrwallingford.co.uk (J.S. Damgaard).
[1] Fax: +44 971 4 26976283.

0378-3839/$ - see front matter © 2005 Elsevier B.V. All rights reserved.
doi:10.1016/j.coastaleng.2005.04.003

with sinusoidal waves, and current with asymmetric waves.

A number of formulae for bedload transport by a steady current exist, originally for application in rivers. Soulsby (1997) lists eight of these, all of a somewhat similar form, by Meyer-Peter and Müller, Bagnold, Van Rijn, Yalin, Madsen, Ashida and Michiue, Wilson and Nielsen. In addition, the widely used bedload formula of Engelund and Fredsøe (1976) should be mentioned.

They can all be written in the general form:

$$\Phi = \mathrm{func}(\theta, \theta_{cr}) \tag{1}$$

where

$$\Phi = \frac{q_b}{\left[g(s-1)d^3\right]^{\frac{1}{2}}} = \text{dimensionless bedload transport rate} \tag{2}$$

$$\theta = \frac{\tau_0}{g\rho(s-1)d} = \text{Shields parameter} \tag{3}$$

θ_{cr}	value of θ at threshold of motion
q_b	volumetric bedload transport rate per unit width
g	acceleration due to gravity
ρ	water density
s	ratio of densities of sediment and water
d	grain diameter
τ_0	bed shear-stress

The grain diameter d is assumed to be uniform in the derivations that follow. In practical applications it can be equated with the median grain diameter, d_{50}. Most of the existing formulae give Φ increasing with $\theta^{3/2}$ for large θ, and some do, and others do not, include a threshold criterion θ_{cr}. Similar non-dimensionalisations are used in the derivations of transport under currents with sinusoidal and asymmetrical waves.

Bedload transport is often considered in two stages: "conventional" bedload occurring over a rippled sand bed in the range of flow conditions $\theta_{cr} \leq \theta \lesssim 0.8$, and sheet flow occurring for $\theta \gtrsim 0.8$ when ripples are washed out and the flat bed moves as a slurry in a layer typically a few millimetres thick. For gravel, the grains are too coarse to form ripples and only the flat-bed condition applies. We hypothesise here that bedload *only* occurs as sheet flow, and that in the case of rippled sand the grains move as a thin sheet-flow layer over the ripple forms, and cause the migration of the ripples. Thus the analysis applies to bedload transport at all current speeds above the threshold of motion and for both flat and rippled beds. While this approach possibly misrepresents the rolling and hopping of grains at low flow speeds, data indicates that there is no distinction in the plot of Φ versus θ between conventional bedload and sheet flow.

Much of the pioneering work on sheet flow was undertaken by K.C. Wilson, and a paper by Pugh and Wilson (1999) summarises both recent thinking and earlier work dating back to 1966. The present paper adopts a similar approach to that of Wilson. It also has similarities with the work of Sleath (1995), although different assumptions are made here. Some of the work reported here dates back to 1992, and some of the formulae were quoted (without derivation) by Soulsby (1997). The present paper gives the underlying derivation of the formulae, and tests them against data from various sources.

A comprehensive review of sheet-flow modelling was given by Kaczmarek (1999), and is not repeated here.

2. Steady current

The bedload transport rate is obtained by taking expressions for the variation with height (z) of the velocity (U) and sediment volume concentration (C) within the sheet-flow layer of thickness S, multiplying them together to form a sediment flux profile (UC) and integrating this vertically through the sheet-flow layer. This is illustrated in Fig. 1. The origin of height ($z=0$) lies at the top of the highest layer of immobile grains.

Within the sheet-flow layer there is a complex interplay between grain–grain interaction and grain–water interaction. These can be represented by sophisticated constitutive relationships (see e.g. Kaczmarek, 1999), but for the present purpose of deriving a simple formulae we follow Wilson and use empirical algebraic relationships.

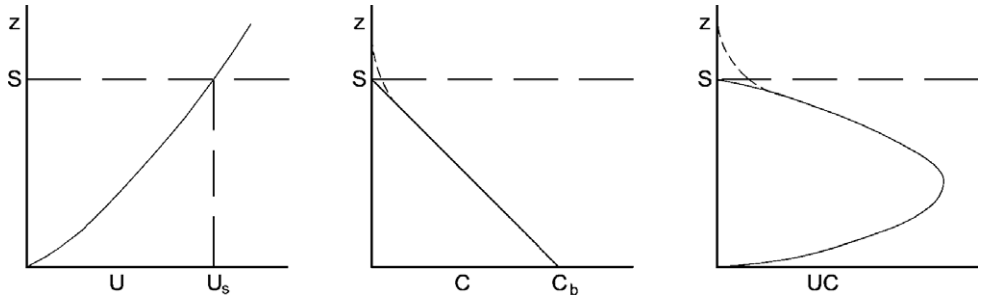

Fig. 1. Schematic profiles of velocity, concentration and sediment flux through the sheet-flow layer.

Pugh and Wilson (1999) showed that the concentration profile measured in their experiments with sand and bakelite grains decreased approximately linearly with z from the constant value C_b within the immobile bed (typically C_b=0.60 to 0.65) to a value of about C=0.05, above which it decreased more slowly as a "tail". The linear decrease is illustrated in Fig. 1 by the solid line, and the tail by the dashed curve. The height S of the sheet-flow layer can be defined by the height at which the linear profile extrapolates back to C=0. The concentration profile is thus given by:

$$C(z) = C_b\left(1 - \frac{z}{S}\right) \tag{4}$$

For our purposes, we will regard the transport of sediment in the "tail" as being suspended load. Sumer et al. (1996) made measurements using sand and plastic grains, and found a similar linear decrease in C except that they found $C_b \simeq 0.32$ at the lowest level of moving grains. They regarded this as being the highest concentration at which grains are sufficiently dilated that they can move past each other.

Having defined the effective height S of the sheet-flow layer, the velocity at this height is denoted as U_s. The velocity profile can then be assumed to take the form:

$$U(z) = U_s f\left(\frac{z}{S}\right) \tag{5}$$

Various expressions have been proposed for the function $f\ (z/S)$. Wilson (1966) took $f\ (z/S) \sim (z/S)^{1/2}$, Sumer et al. (1996) took $f\ (z/S) \sim (z/S)^{3/4}$, and Pugh and Wilson (1999) took $f\ (z/S) = 0.4 + 0.6\ (z/S)$.

The choice is not critical, and we will take the expression for the velocity profile to be:

$$\frac{U(z)}{U_s} = \left(\frac{z}{S}\right)^n \tag{6}$$

where n is a power between 0.5 and 1. Further, we will assume that the velocity U_s at the top of the sheet-flow layer is proportional to the friction velocity $u* = (\tau_0/\rho)^{1/2}$.

$$U_s = A_1 u_* \tag{7}$$

The coefficient A_1 has been calculated variously from data as: 8.2 (Wilson, 1989), 9.4 (Pugh and Wilson, 1999) and 16.1 (deduced from Sumer et al., 1996). Since the depth-averaged current speed over the whole water depth is typically about (20–30)u_* in rivers and shallow seas, it can be seen that the velocity at the top of the sheet-flow layer is roughly half the depth-averaged value.

The thickness S of the sheet-flow layer can be written in terms of known variables by assuming Coulomb friction, so that the shear-stress at the bottom of the moving layer of grains is proportional to the (submerged) weight of grains supported. We assume that the relevant friction is the shear-stress $(\tau_0 - \tau_{cr})$ in excess of the threshold shear-stress τ_{cr} for motion of the grains. This ensures that transport is zero for $\tau \le \tau_{cr}$, a condition sometimes neglected in sheet-flow work where usually $\tau \gg \tau_{cr}$. Coulomb friction is thus expressed by:

$$(\tau_0 - \tau_{cr}) = \mu g \rho (s-1)\frac{C_b}{2} S \tag{8}$$

where μ is the coefficient of dynamic friction and $C_b/2$ is the mean volume concentration through the sheet-flow layer. Re-arranging Eq. (8) gives:

$$S = \frac{2(\tau_0 - \tau_{cr})}{\mu g \rho (s-1) C_b} \tag{9}$$

The volumetric sediment transport rate is given by the integral of the flux through the sheet-flow layer:

$$q_b = \int_0^S U(z)C(z)\mathrm{d}z \tag{10}$$

Substituting from Eqs. (4), (6) and (7) and integrating gives:

$$q_b = \frac{A_1 C_b u_* S}{(n+1)(n+2)} \tag{11}$$

Substituting for S from Eq. (9) gives:

$$q_b = \frac{2A_1}{(n+1)(n+2)\mu} \frac{u_*(\tau_0 - \tau_{cr})}{g\rho(s-1)} \tag{12}$$

This can be non-dimensionalised by making use of the definitions of Φ and the Shields parameter θ (Eqs. (2) and (3)) to give:

$$\Phi = A_2 \theta^{1/2}(\theta - \theta_{cr}) \tag{13}$$

where

$$A_2 = \frac{2A_1}{(n+1)(n+2)\mu} \tag{14}$$

To evaluate A_2, we first note that the bed concentration C_b has cancelled out so its value is irrelevant, and then take typical values of A_1=9, n=0.75, and

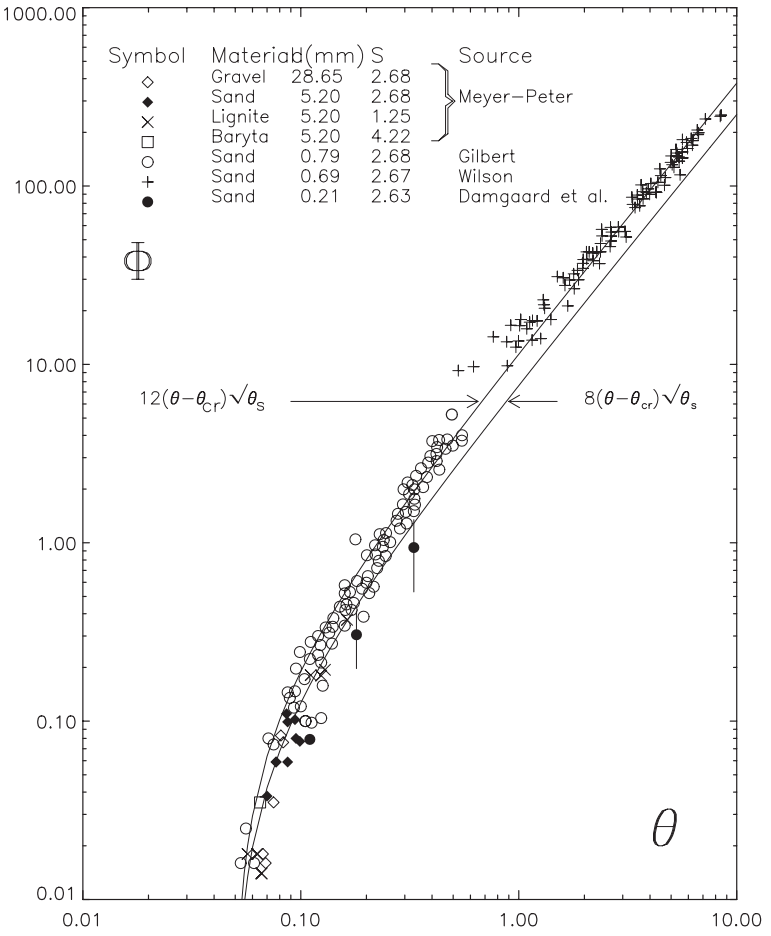

Fig. 2. Comparison of Eq. (13) with data, for A_2=8 and 12 and θ_{cr}=0.05.

μ=0.5 tan 32°, where 32° is a typical static friction angle for sand (angle of repose) and the factor 0.5 between dynamic and static friction is given by Madsen (1991). These values yield A_2=12.0, so that the non-dimensional bedload transport rate is given by:

$$\Phi = 12\theta^{1/2}(\theta - \theta_{cr}) \quad (15)$$

This is the expression given by Soulsby (1997), and is identical to a formula derived earlier via a different route by Nielsen (1992). We note the similarity with the sheet-flow formula of Wilson (1966):

$$\Phi = 12\theta^{3/2} \quad (16)$$

Wilson's arguments were similar, but not identical, to the ones used here, and he neglected the threshold term θ_{cr}. The widely used Meyer-Peter and Müller (1948) formula is also similar:

$$\Phi = 8(\theta - 0.047)^{3/2} \quad (17)$$

The difference between the coefficient 12 in Eqs. (15) and (16) and 8 in Eq. (17) is explained if we look at the range of variability in the calculation of A_2. Recalling the range of values of A_1, n and μ discussed earlier, if we take A_1=8, n=1 and μ=0.65 then A_2=4.1, whereas taking A_1=16, n=0.5 and μ=0.3 yields A_2=28. Since all these coefficients depend to some extent on factors such as the shape, angularity, and degree of sorting of the grains, it seems possible that different sediments may have different values of A_2. This particularly applies to the difference between plastic grains and natural sands and gravels. A comparison with a wide range of data is shown in Fig. 2 using both A_2=8 and 12, together with a value of θ_{cr}=0.05 which is typical of the sediments plotted. It is seen that the curve with A_2=12 fits better with Wilson's data at large θ, whereas the curve with A_2=8 fits the data for smaller θ better. The data of Damgaard et al. (1997) for bedload transport of sand in a duct (Fig. 2) also gives a better fit with a coefficient of 8 than with 12. The goodness-of-fit to the data is equal for A_2=8 and 12, namely that 91% of predictions lie within a factor-of-2 of the data, and 100% within a factor-of-5, for both values of the coefficient. Some element of fitting of the coefficient to specific sediments may thus be desirable. However, a factor of 1.5 is not a large uncertainty in terms of sediment transport formulae.

The good fit of the formula to the data throughout the range $0.05<\theta<8$ seen in Fig. 2, and the lack of a distinct break in the data between rippled-bed and sheet-flow cases, is taken as justification of the hypothesis that bedload transport over ripples can be treated in the same way as sheet flow. Alternatively, when the model is used outside the parameter range relevant to sheet flow, it may be taken simply as an empirical model equivalent to the model of Nielsen (1992).

3. Current plus sinusoidal waves

The bedload transport beneath a sinusoidal wave on its own is symmetrical, and hence the net transport is zero. Consequently, we will not consider this case. In this section the transport by a steady current superimposed on sinusoidal waves is derived, and in the next section the case of a steady current superimposed on asymmetrical waves is considered. The case of asymmetrical waves alone, which do produce a net transport, is a special case of the latter.

Madsen (1991) derived an expression for the response time of a grain to a sudden change in the flow and concluded that bedload transport responds virtually instantaneously compared to the timescale of coastal wave motions. We therefore adopt the steady-current formula, Eq. (13), and apply it in a quasi-steady fashion at each instant through a wave cycle. For mathematical simplicity, and again following Madsen (1991), we assume that the bed shear-stress is the vector sum of a steady component due to the current and a sinusoidally varying component due to the wave. The wave is taken to propagate in a direction ϕ relative to the current direction.

$$\vec{\tau_0}(t) = \vec{\tau_m} + \vec{\tau_w}\cos\omega t \quad (18)$$

where
$\vec{\tau_0}(t)$ = time-varying bed shear-stress vector;
$\vec{\tau_m}$ = mean of $\vec{\tau_0}$ over a wave cycle;
$\vec{\tau_w}$ = amplitude of wave-induced bed shear-stress vector; ω=radian wave frequency; t=time

The following points may be made in connection with the above approach:

a. The effects of wave-induced pressure-gradient and inertia effects on the grains have been

neglected. The importance of these forces relative to the submerged weight of the grain is given by $U_w\omega/g(s-1)$, where U_w is the wave orbital velocity amplitude at the bed (Sleath, 1994). The effects become noticeable if this ratio exceeds 0.12 (Zala Flores and Sleath, 1998), which could easily occur for low density sediments (e.g. plastics) under laboratory waves. However, natural sediments and waves in the sea will not generally exceed 0.12, so these effects can justifiably be ignored in practical applications.

b. Conventionally, the wave-induced orbital velocity would vary sinusoidally, so that a quadratic friction law would give a time variation of the bed shear-stress going as $\cos\ \omega t\ |\cos\ \omega t|$. The difference from the mathematically simpler form used in Eq. (18) is not thought to be important for the net bedload transport. The error in the net transport, estimated by comparing the integrals through half a wave-cycle of $(\cos\ \omega t)^{3/2}$ and $\cos^3\ \omega t$, is at most 32%, and will generally be smaller. Furthermore, direct measurements of turbulent bed shear-stresses due to sinusoidal waves (Simons et al., 1993; Lodahl et al., 1998) appear visually to conform more nearly to a sinusoidal than a quadratic time dependence.

c. The mean bed shear-stress under combined wave-and-current is larger than that under the same current alone (see Soulsby, 1997).

d. Most wave-current interaction models indicated that the magnitude of the oscillatory part of the stress $|\vec{\tau_w}|$, would be larger than that due to the same wave alone. However, experiments indicate that this non-linear enhancement is not observed (Simons et al., 1993).

e. A number of alternative implicit and numerical methods of calculating the mean and oscillatory shear-stresses due to combined wave and current flows have been proposed, some of which are listed by Soulsby (1997, p. 90). In addition, a new explicit method (for both rough and smooth flows) has been developed by Soulsby and Clarke (2004).

The expression derived for transport by a current alone (Eq. (13)) can be expressed in vector form, with the x-axis aligned with the current direction, to account for the variation in bedload transport direction during a wave cycle:

$$\vec{\Phi} = A_2\theta^{1/2}(\theta-\theta_{cr})\frac{\vec{\theta}}{\theta} \tag{19}$$

where: $\vec{\Phi} = (\Phi_x, \Phi_y)$ is the vector dimensionless bedload transport rate; $\vec{\theta} = \frac{\vec{\tau_0}}{g\rho(s-1)d}$ is the vector Shields parameter; $\theta = |\vec{\theta}|$.

Similarly the modulus of the time-mean Shields parameter, $\theta_m = |\vec{\theta_m}|$, and the amplitude of the oscillatory part of the Shields parameter, $\theta_w = |\vec{\theta_w}|$, are defined from nondimensionalising $\vec{\tau_m}$ and $\vec{\tau_w}$.

The time-mean vector bedload transport rate $\langle\vec{\Phi}\rangle$ over a wave cycle is given by

$$\langle\vec{\Phi}\rangle = \frac{A_2}{2\pi}\int_0^{2\pi}\theta^{1/2}(\theta-\theta_{cr})\frac{\vec{\theta}}{\theta}\mathrm{d}(\omega t) \tag{20}$$

Values of $\langle\vec{\Phi}\rangle$ can be calculated by numerical integration of Eq. (20), by calculating $\vec{\theta}$ using Eq (18) over a large number of intervals in one wave cycle for specified inputs of θ_m, θ_w, θ_{cr} and ϕ. Results of such an integration, with 200 intervals per wave cycle, are shown as the curves in Fig. 3 for the case $\theta_{cr}=0.04$, $\phi=45^\circ$ and a range of values of θ_m and θ_w. The x-component Φ_x (Fig. 3a) shows that the transport parallel to the current is enhanced by the wave action (compared to the current-only curve) by an amount that increases with θ_w and decreases with θ_m. At $\theta_m=10^{-2}$, waves with $\theta_w \geq 10^{-1}$ mobilise the sediment so that it is transported when the current alone is too weak to move it. At $\theta_m=10^{-1}$, the strongest wave ($\theta_w=10^2$) increases the transport rate to 100 times the value due to the current alone, but when $\theta_m=10^2$ even the strongest wave has but little effect in enhancing the current-alone transport. (Of course, values of θ_m or θ_w as large as 100 will not normally occur in natural flows, but the results are included to illustrate the general behaviour.)

There is also a non-zero component of the transport, Φ_y, normal to the current direction in cases where $\phi\neq 0^\circ$ or 90°. This occurs due to the nonlinear relationship of bedload transport to stress, because the magnitude of the resultant stress is larger in the half-cycle when the wave complements the current than in the half-cycle when the wave opposes the current. Fig. 3b shows Φ_y for the case $\theta_{cr}=0.04$, $\phi=45^\circ$ and a

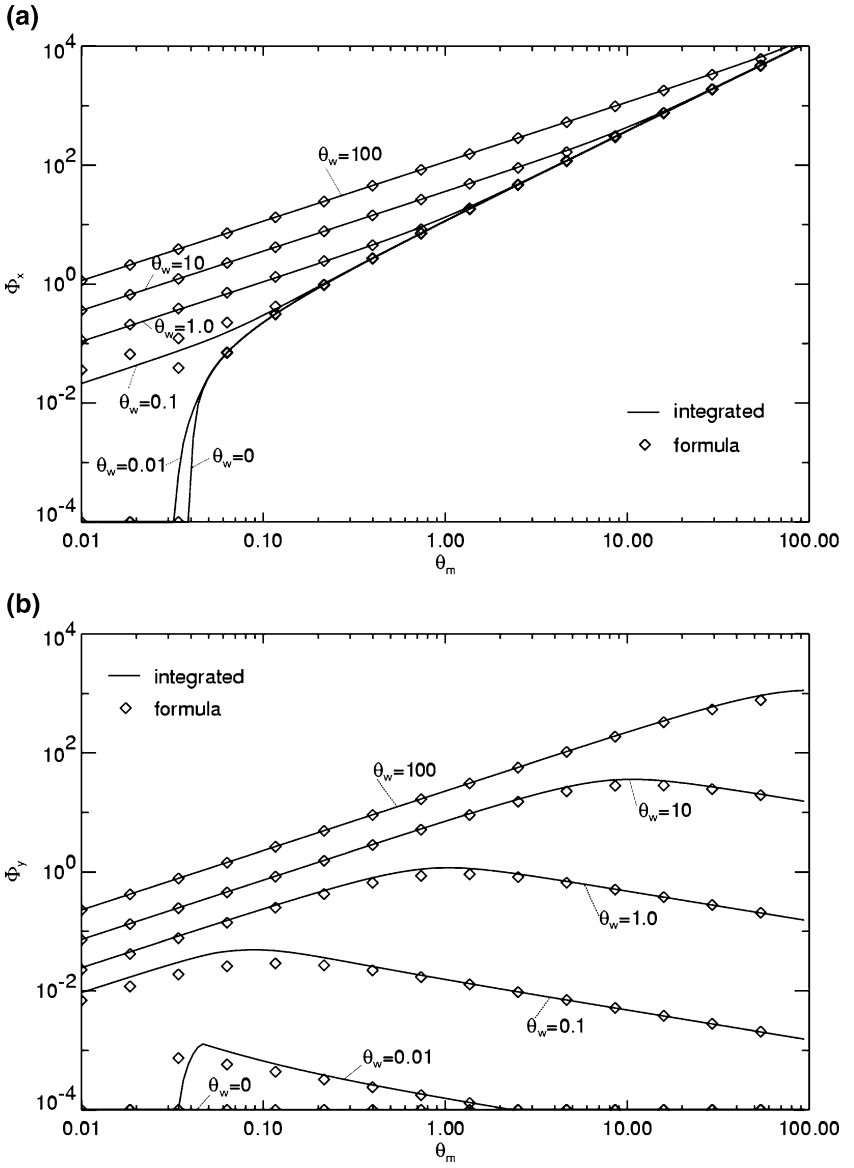

Fig. 3. Bedload transport by combined current and sinusoidal waves, (a) x-component (aligned with current), (b) y-component. Curves: by numerical integration; symbols: from Eqs. (23)–(28) with A_2=12.

range of θ_m and θ_w. The magnitude is zero for θ_w=0 (current only case) and increases with θ_w for a given value of θ_m. There is a maximum of θ_w with respect to θ_m, generally in the vicinity of θ_w=θ_m. The size of Φ_y is largest for ϕ=45°, decreasing to zero at ϕ=0° and 90°. The y-component of transport takes values up to about 20% of the x-component, so that the direction of transport can be up to about 11° different to the current direction. The sense is such that if waves are approaching a coast at an angle and driving a long-shore current parallel to the coast, there will be a component of bedload transport carrying sediment onshore. This may be a factor in determining the steepness of beach profiles. This directional deviation may be compared with the deviation of up to 20° (in the same sense, and for a similar reason) predicted

theoretically by Grant and Madsen (1979) for the direction of the mean bed shear-stress in a wave-plus-current flow compared with the current direction outside the wave boundary layer.

Algebraic approximations to the curves shown in Fig. 3 have been derived for ease of use in practical applications. The derivation of algebraic approximations for the net transport by a steady current superimposed on *asymmetrical* waves was presented in detail by Soulsby and Damgaard (2005). A summary of the derivation of the transport by a current plus sinusoidal waves is given here; the full derivation can be obtained by setting the second harmonic to zero in the derivation by Soulsby and Damgaard (2005).

Two limiting cases are derived using perturbation analysis: a weak wave superimposed on a strong current, and a weak current superimposed on a strong wave. Subsequently the two cases are combined, and results compared to the full integrations shown in Fig. 3. In the first case expansions are made in terms of the perturbation parameter $\delta=\theta_w/\theta_m$, and in the second case in terms of $\varepsilon=\theta_m/\theta_w$. Terms of order δ^2 and ε^2 respectively are neglected. For mathematical tractability the threshold term is omitted initially ($\theta_{cr}=0$), and re-introduced subsequently.

For the current-dominated case ($\delta \ll 1$), the analytical integration of Eq. (20) with $\theta_{cr}=0$ yields:

$$\Phi_{x1} = A_2\theta_m^{3/2}$$

$$\Phi_{y1} = \frac{A_2}{8}\theta_m^2\theta_m^{-1/2}\sin 2\phi \tag{21}$$

Similarly, for the wave-dominated case ($\varepsilon \ll 1$), integration yields:

$$\Phi_{x2} = A_2(0.9534 + 0.1907\cos 2\phi)\theta_w^{1/2}\theta_m$$

$$\Phi_{y2} = A_2\left(0.1907\theta_m\theta_w^{1/2}\sin 2\phi\right) \tag{22}$$

Comparisons with the numerically integrated curves in Fig. 3 show that Φ_{y1} and Φ_{y2} can be merged analytically, but a better fit for Φ_x is obtained by taking the maximum of Φ_{x1} and Φ_{x2}. The resulting expressions (with θ_{cr} replaced) are:

$$\Phi_{x1} = A_2\theta_m^{1/2}(\theta_m - \theta_{cr}) \tag{23}$$

$$\Phi_{x2} = A_2(0.9534 + 0.1907\cos 2\phi)\theta_w^{1/2}\theta_m \tag{24}$$

$$\Phi_x = \max(\Phi_{x1}, \Phi_{x2}) \tag{25}$$

$$\Phi_y = \frac{A_2\left(0.1907\theta_m\theta_w^2\sin 2\phi\right)}{\theta_w^{3/2} + (3/2)\theta_m^{3/2}} \tag{26}$$

$$\text{subject to:}\quad \Phi_x = \Phi_y = 0 \ \text{ if } \ \theta_{max} \leq \theta_{cr} \tag{27}$$

$$\text{where:}\quad \theta_{max} = \left[(\theta_m + \theta_w\cos\phi)^2 + (\theta_w\sin\phi)^2\right]^{1/2} \tag{28}$$

Eqs. (23)–(28) are the results that were quoted without derivation in Soulsby (1997), with $A_2=12$. As seen earlier, the value of A_2 may vary between 8 and 12 depending on the sediment properties. The symbols in Fig. 3 show values calculated using Eqs. (23)–(28). It is seen that in general they lie very close to the curves obtained by numerical integration. Exceptions occur for cases where both θ_m and θ_w are close to threshold. For the case $\theta_w=0.1$, and for $\theta_m<0.3$, the approximations lie within a factor of 1.8 from the full solution, but in all other cases the agreement is much better. In view of the assumptions (a) to (d) made in deriving the full solution, the algebraic approximation is acceptable, and is much faster computationally than performing the integration numerically.

Laboratory measurements of the net bedload transport of sand of various sizes by a sinusoidal wave superimposed normal to a current were made by Lee-Young (1988). The data were tabulated for the present purposes by Soulsby and Damgaard (2005).

Predictions using Eqs. (23)–(28) with $A_2=12$, give reasonable agreement with the data (Fig. 4). It is found that 47% of the predictions lie within a factor-of-2, 85% within a factor-of-5, and 98% within a factor-of-10 of the data. Although the agreement is less good than for the current-alone case, it is reasonable for the more complicated case with waves included. There is some indication in Fig. 4 that either the predictions under-estimate for fine grains and over-estimate for coarse grains, or that they under-estimate low transports and over-estimate high transports. A possible explanation is that the measurements with Sand A (d=0.203 mm) contain a contribution due to suspended transport. If this is so, then a value

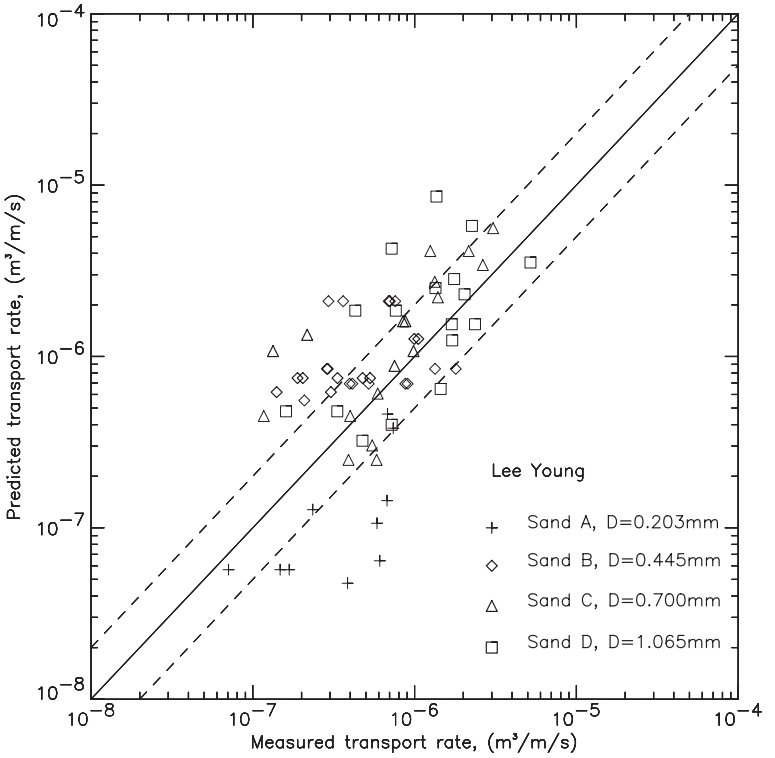

Fig. 4. Comparison of Eqs. (23)–(28) with data, for A_2=12.

of the coefficient A_2=8 would improve the fit for all the data since the coarser grains (d=0.445 to 1.065 mm) are less likely to be suspended.

4. Current plus asymmetric waves

In the preceding section, the oscillatory component of the shear stress was assumed to vary as a single harmonic. A direct consequence of this assumption is that the forces generated are completely symmetrical throughout a wave cycle: a sediment grain resting on the seabed cannot "feel" the direction of wave propagation. However, as the wave shoals it becomes increasingly asymmetric with higher orbital velocities under the crest and lower orbital velocities under the troughs. This wave asymmetry is an important sediment transporting factor. In order to include the effect of wave and force asymmetry in the present model, a second harmonic has been added to the oscillatory component of the shear stress. The phase-shift between the first and the second harmonic is set to -π/2. The resulting oscillatory shear stress is (see Fig. 5):

$$\theta_w(\omega t) = \theta_w\left[\sin(\omega t) + \Delta\sin\left(2\omega t - \frac{\pi}{2}\right)\right] = \theta_w\Omega(\omega t) \quad (29)$$

in which

$$\Delta = \frac{\theta_{w,2}}{\theta_w} \quad (30)$$

is the ratio between the amplitude of the second harmonic, $\theta_{w,2}$, and the amplitude of the basic harmonic, θ_w. Only values of $\Delta \leq 0.2$ are considered, since larger values give an unrealistic local maximum of $\Omega(\omega t)$ in the trough. The variation of $\Omega(\omega t)$ over a cycle is shown in Fig. 5b for various values of Δ.

The magnitude of Δ can be estimated by using Stokes' 2nd order theory (e.g. Fredsøe and Deigaard, 1992) to obtain the second harmonic for the velocity. The present authors found this gave good agreement with data in a confidential consultancy study. This can be converted to Δ through the quadratic friction law,

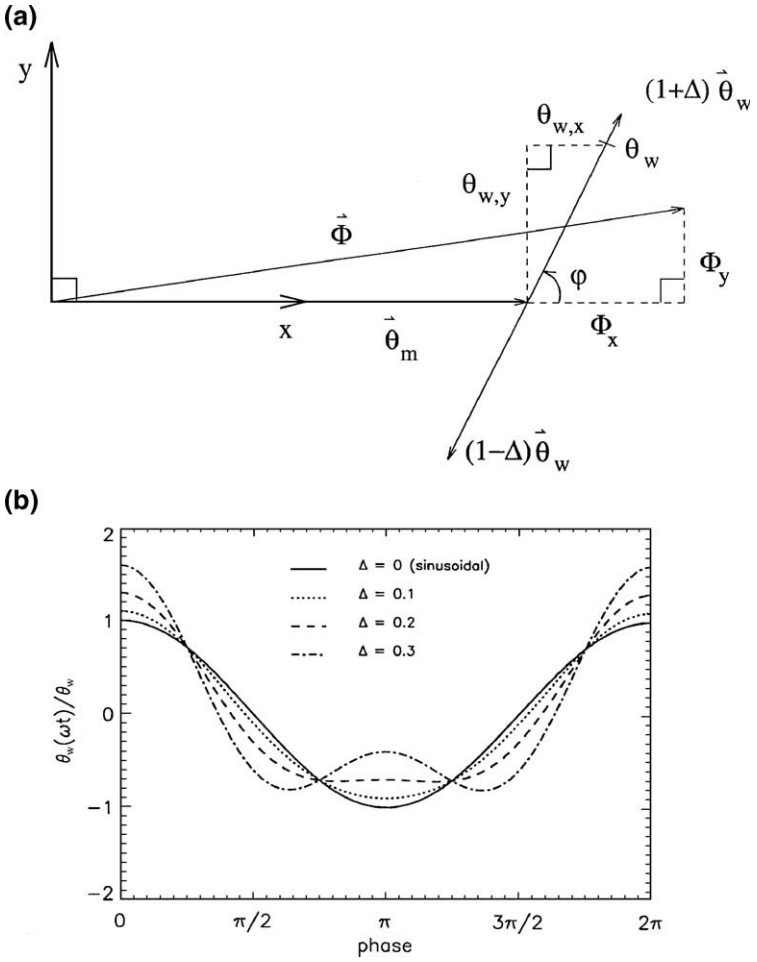

Fig. 5. (a) Sketch of notations for shear-stress and transports for current plus asymmetric waves. (b) Variation of asymmetric bed shear-stress through a wave-cycle, for various strengths of second harmonic.

which for present purposes governs the magnitude (though not the time dependence) of the bed shear stress.

Algebraic approximations to the non-dimensional bedload transport vector resulting from a shear stress varying as in Eq. (29) were derived by Soulsby and Damgaard (2005). The methodology follows that given in the preceding section, but with the added complication of the second harmonic. The resulting expressions (to order Δ) are:

$$\Phi_{x1} = A_2\theta_m^{1/2}(\theta_m - \theta_{cr}) \tag{31}$$

$$\Phi_{x2} = A_2(0.9534 + 0.1907\cos 2\phi)\theta_w^{1/2}\theta_m + A_2(0.229\Delta\theta_w^{3/2}\cos\phi) \tag{32}$$

$$\Phi_x = \max(\Phi_{x1}, \Phi_{x2}) \tag{33}$$

$$\Phi_y = A_2\frac{(0.1907\theta_w^2)}{\theta_w^{3/2} + (3/2)\theta_m^{3/2}}(\theta_m \sin 2\phi + 1.2\Delta\theta_w \sin\phi) \tag{34}$$

subject to: $\Phi_x = \Phi_y = 0$ if $\theta_{max} \leq \theta_{cr}$ (35)

where: $\theta_{max} = \max\{\theta_{max1}, \theta_{max2}\}$ with:

$$\theta_{max1} = \sqrt{[\theta_m + \theta_w(1+\Delta)\cos\phi]^2 + [\theta_w(1+\Delta)\sin\phi]^2}$$

$$\theta_{max2} = \sqrt{[\theta_m + \theta_w(1-\Delta)\cos(\phi+\pi)]^2 + [\theta_w(1-\Delta)\sin(\phi+\pi)]^2}$$

It is seen that the asymmetry results in an additional net transport in the current direction (Φ_{x2}) if $0<\phi<\pi/2$, and a reduction if $\pi/2<\phi<\pi$, compared to the symmetrical case. The net transport normal to the current direction is also increased in the direction of wave propagation. If $\Delta=0$ the equations reduce to the symmetrical case.

The special case of asymmetric waves without a current is obtained by setting $\theta_m=0$ in either Eq. (32) or (34). The resulting net transport due to asymmetrical waves alone is:

$$\Phi = A_2\left(0.229\Delta\theta_w^{3/2}\right) \tag{36}$$

The transport is proportional to the strength Δ of the second harmonic of bed shear-stress, and is directed along the wave propagation direction. This approach is more rigorous than earlier approaches based on calculating the difference between the half-cycle transports under the crest and trough of the wave (e.g. Sleath, 1978; Soulsby, 1997, p. 163). The present approach follows the time dependence of the stress more realistically, and hence the predicted net sediment transport is expected to be more accurate.

We are not aware of data for the case of asymmetrical waves with a current, but data for net bedload transport by asymmetric waves alone measured by King (1991) and Al-Salem (1993) are shown in Fig. 6. The data was tabulated for the present purposes by Soulsby and Damgaard (2005). Eq. (36) with $A_2=12$ is seen to give reasonable agreement with the data, with 62% of predictions lying within factor 2 of the data and 87% within factors of 5 and 10. Note that 4 data points in which the transport was against the wave direction are not shown in Fig. 6, which comprise the remaining 13% within factors 5 and 10. Such cases are not catered for by the present formulation, since negative transport is usually attributed to vortex-induced suspension of sand over a rippled bed.

Other second order effects may also influence the sediment transport, principally the effect of

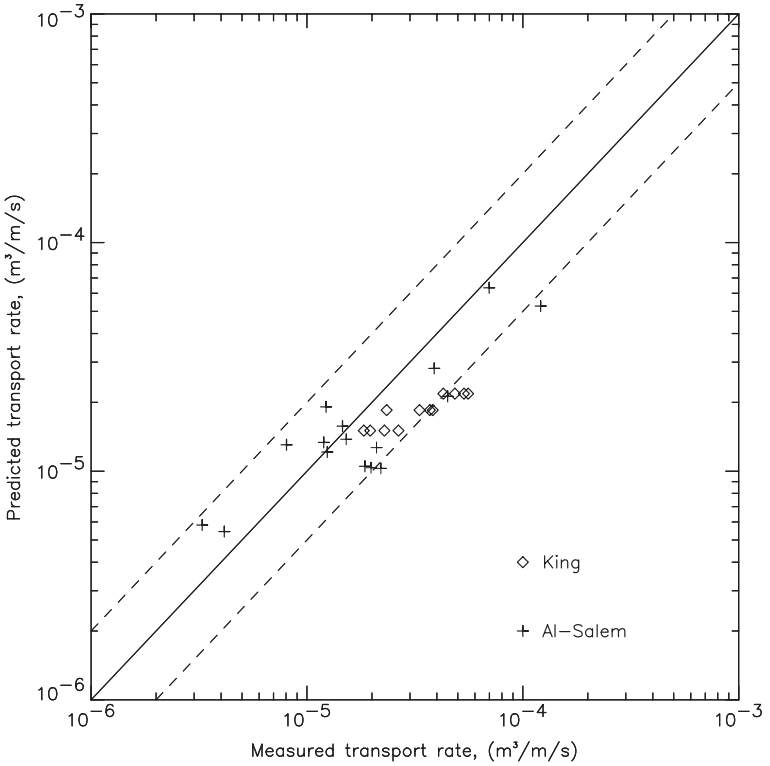

Fig. 6. Comparison of Eq. (36) with data, for $A_2=12$.

wave boundary layer streaming (see, for example, Fredsøe and Deigaard, 1992). The relative effects of asymmetry and streaming on bedload transport were compared by Myrhaug et al. (in press). They showed that the effect of asymmetry is much more important than streaming in shallow water, but becomes smaller than streaming in intermediate depths. The effect of streaming could be included in the present formulation by adding it to the current.

5. Longshore transport

One of the commonest requirements for calculations of sediment transport in coastal waters is the estimation of the longshore sediment transport (littoral drift) on beaches. On shingle beaches this is due almost entirely to bedload transport, yet the most commonly used approach, the CERC (1984) formula, is calibrated for sand beaches where the dominant mode of transport is suspension. Here we derive a formula designed specifically for longshore bedload transport, with application to shingle beaches principally in mind. This approach was reported previously by Damgaard and Soulsby (1997), and only a summary is given here.

The approach is based on the use of Eqs. (23)–(28) for the bedload transport by (symmetrical) waves plus a current at all points along a beach-normal passing through the surf zone. For mathematical simplicity the expression for symmetrical waves is used, since the additional terms for asymmetrical waves are expected to have only a small effect on the longshore transport. It is conventional for the longshore transport rate to be expressed as the transport integrated along the beach-normal transect.

The procedure of derivation for the analytical formula is as follows: Approximate expressions for the mean bottom shear-stresses, required as input to the bedload transport formula are derived directly from the depth-integrated momentum equation. This avoids the need to calculate the speed of the longshore current. In order to solve the momentum equation analytically a number of assumptions have been made.

i) The ratio of wave-height, H_b, and water depth, h_b, at the breaker point is constant, $H_b/h_b=\gamma_b=0.8$.
ii) After breaking the wave-height decays linearly, so that $H=\gamma_b h$.
iii) No further refraction takes place beyond the breaking point, i.e. the angle of wave incidence, α, is constant in the surf zone, $\alpha(y)=\alpha_b$.
iv) All waves break at the same location.
v) Shallow-water linear wave theory is used in the surf zone.
vi) The effect of a lateral bed slope on the sediment transport is neglected.
vii) The effect of cross-shore currents (e.g. undertow) on the longshore transport is neglected.
viii) The variation in mean water level (set-down and set-up) is ignored.

The effect of some of these assumptions will be to increase, and of others to decrease, the predicted integrated transport. Their combined effect is parameterised by introducing an additional multiplicative constant, A_3, into the transport formula. The mean value of A_3 is then determined by comparison with field data.

The beach is assumed to be plane with a constant slope, $\tan\beta$. Ignoring the lateral transfer of turbulent momentum the depth-integrated momentum equation for a longshore uniform beach reduces to a balance between the cross-shore gradient of the shear component of the radiation stress and the bottom friction:

$$\frac{\partial S_{xy}}{\partial y} = -\tau_{b,x} \tag{37}$$

where S_{xy} is the shear component of the radiation stress and $\tau_{b,x}$ is the longshore component of the bed shear stress. The relation between φ and α_b is $\varphi=(\pi/2)-\alpha_b$. The radiation stress can be expressed in terms of the momentum flux, F_m, in the direction of wave propagation:

$$S_{xy} = F_m \cos(\alpha)\sin(\alpha) \tag{38}$$

in which α is the angle of wave incidence and F_m is determined according to linear wave theory as:

$$F_m = \frac{1}{8}\rho g H^2 \tag{39}$$

Combining Eqs. (37)–(39) yields an expression for τ_b

$$\tau_b = -\frac{1}{16}\rho g \frac{\partial}{\partial y}\left(\sin(2\alpha)H^2\right) \tag{40}$$

According to the assumptions employed regarding refraction and wave height decay, (40) reduces to:

$$\tau_b = -\frac{1}{16}\rho g \sin(2\alpha_b) 2H \frac{\partial H}{\partial y} = \frac{\gamma_b}{8}\rho g H \sin(2\alpha_b)\tan\beta \tag{41}$$

in which h is the depth and γ_b is the constant ratio between wave height and depth in the surf zone. Thus the shore parallel component of the mean Shields parameter can be expressed as:

$$\theta_{m,x} = \frac{\gamma_b H \sin(2\alpha_b)\tan\beta}{8(s-1)d} \tag{42}$$

Expressions for the oscillatory shear-stress, θ_w, are derived by making the following assumptions (see Damgaard and Soulsby, 1997, for details):

i) The oscillatory bed shear-stress is based on a quadratic friction law utilising a wave friction factor, f_w,
ii) for sediment transport in the range $\theta_{cr} \leq \theta \lesssim 0.8$, the wave friction factor, $f_{w,r}$, takes the form given by Soulsby (1997, Eq. (62a)) for rough turbulent flows,
iii) for sheet flow conditions ($\theta \gtrsim 0.8$) the wave friction factor, $f_{w,s}$, takes the form given by Wilson (1989),
iv) the choice of friction factor is determined by the maximum of $f_{w,r}$ and $f_{w,s}$,
v) the friction factor is not enhanced by the presence of a near-normal incidence current, in accord with experimental observations of Simons et al. (2001),
vi) some simplifications are made to the expressions for mathematical convenience.

These assumptions yield expressions for θ_w given by the maximum of:

$$\theta_{w,r} = \frac{\sqrt{2}}{8} g^{-1/4} \frac{(\gamma_b H)^{3/4}}{(s-1)\sqrt{dT}} \tag{43}$$

and

$$\theta_{w,sf} = 8.187 \cdot 10^{-3} g^{-1/5} (\pi(s-1)T)^{-2/5} \frac{(\gamma_b H)^{6/5}}{(s-1)d} \tag{44}$$

Now the current-dominated case of the dimensionless bed-load transport rate is calculated by inserting Eq. (42) into Eq. (23)

$$\Phi_{x1} = \frac{A_4}{8^{3/2}} \left(\frac{\gamma_b H \tan\beta}{(s-1)d}\right)^{3/2} \left(\sin(2\alpha_b) - \theta^*_{cr}\right)\sqrt{|\sin(2\alpha_b)|} \tag{45}$$

where

$$\theta^*_{cr} = \theta_{cr} \frac{8(s-1)d}{\gamma_b H \tan\beta} \tag{46}$$

and $A_4=A_2A_3$, where A_2 is the coefficient between 8 and 12 introduced in Section 2 and A_3 is the calibration coefficient. The wave-dominated case (subject to flow regime) is determined by inserting Eqs. (42) and (43) or (44) into Eq. (24)

$$\Phi_{x2,r} = A_4(0.05011 + 0.01002\cos(2\varphi))\frac{(\gamma_b H)^{11/8}\tan\beta\sin(2\alpha_b)}{g^{1/8}d^{5/4}T^{1/4}(s-1)^{3/2}} \tag{47}$$

or

$$\Phi_{x2,sf} = A_4(0.01078 + 0.002157\cos(2\varphi))\frac{(\gamma_b H)^{8/5}\tan\beta\sin(2\alpha_b)}{g^{1/10}d^{3/2}(\pi T)^{1/5}(s-1)^{17/10}} \tag{48}$$

In order to transform to a bulk transport formula, Eqs. (45), (47) and (48 are integrated across the surf zone, using assumptions i) and ii) above for the decay of wave height through the surf zone:

$$\int_{\text{surf zone}} \Phi_x \mathrm{d}y = \int_{H_b}^{0} \Phi_x \frac{1}{\mathrm{d}H/\mathrm{d}y}\mathrm{d}H = \frac{-1}{\gamma_b\tan\beta}\int_{H_b}^{0}\Phi_x \mathrm{d}H \tag{49}$$

The cross-shore integrated volumetric sediment transport rate $Q_{b,1}$ [m^3/s] is given as:

$$Q_{b,1} = \sqrt{g(s-1)d^3}\int_{\text{surf zone}} \Phi \mathrm{d}y \tag{50}$$

and the resulting analytical formula for $Q_{b,1}$ is expressed as a combination of a current-dominated transport (Q_{x1}) and a wave-dominated transport (Q_{x2}):

$$Q_{b,1} = \text{sign}\{\alpha_b\}\max\{|Q_{x1}|, |Q_{x2}|\} \tag{51}$$

$$Q_{x1} = \begin{cases} 0.0175A_4\dfrac{\sqrt{g\gamma_b tan\beta}H_b^{5/2}}{(s-1)}\left(\sin(2\alpha_b) - \dfrac{5}{3}\theta_{cr}^*\right)\sqrt{|\sin(2\alpha_b)|} & \text{for } \sin(2\alpha_b) > \frac{5}{3}\theta_{cr}^* \\ 0 & \text{for } \sin(2\alpha_b) \le \frac{5}{3}\theta_{cr}^* \end{cases} \tag{52}$$

$$Q_{x2} = \begin{cases} A_4(0.0208 + 0.00425\cos(2\varphi))\dfrac{g^{3/8}d^{1/4}\gamma_b^{3/8}H_b^{19/8}}{T^{1/4}(s-1)}\sin(2\alpha_b) & \text{for } f_{w,r}/f_{w,sf} > 1 \\ A_4(0.00417 + 0.00083\cos(2\varphi))\dfrac{g^{2/5}\gamma_b^{3/5}H_b^{13/5}}{(\pi T)^{1/5}(s-1)^{6/5}}\sin(2\alpha_b) & \text{for } f_{w,r}/f_{w,sf} \le 1 \end{cases} \tag{53}$$

subject to the threshold condition

$$Q_{b,1} = 0 \text{ for } \theta_{max} \le \theta_{cr} \tag{54}$$

where

$$\theta_{max} = \sqrt{(\theta_m + \theta_w\cos\varphi)^2 + (\theta_w\sin\varphi)^2} \tag{55}$$

In general the current dominated term, Q_{x1}, is used for large wave heights, small grain sizes and large beach slopes. In most cases $f_{w,r} > f_{w,sf}$. This is especially true for larger grain sizes which are rarely transported as sheet flow. A study of a field data set with approximately 25 000 wave conditions sampled throughout a 4 year

period (Damgaard et al., 1996) showed that Q_{x1} was applied for approximately 60% of the wave conditions, Q_{x2} with $f_{w,r}$ for the remaining 40% of the conditions and Q_{x2} with $f_{w,sf}$ was not applied at all for that particular data set.

The value of the calibration coefficient A_3 was determined by setting $A_2=12$ and comparing the predictions of Eqs. (51)–(55) with 3 years of field data, as described by Damgaard and Soulsby (1997). This comprised 3-hourly wave measurements and repeat beach profile surveys at 2–3 month intervals following re-nourishment of a shingle beach at Seaford on the south coast of England. Best agreement between the predictions and the measurements was obtained by setting $A_3=1/12$. Thus the calibrated value of coefficient $A_4=1.0$.

The analytical formulae developed here (Eqs. (51)–(55)) have advantages over the CERC formula when used for bedload longshore transport in that they were specifically designed for bedload transport of coarse sediments, they contain a threshold term, and they contain dependencies on the grain size, beach slope and wave period. A comparison between the present method and the CERC formula was made by Damgaard and Soulsby (1997). Graphs illustrating the respective dependencies on the various input parameters were presented, although these were made with the pre-calibration version (i.e. $A_4=12$), and the curves marked "analytical model" should be reduced by a factor of 12 to be consistent with the recommended value of $A_4=1.0$. The graphs showed that, compared with the CERC formula, the variation of the longshore transport rate by the new method:

– has much the same power–law dependence on wave height,
– varies with angle of wave incidence in the same way,
– first decreases with wave period, then becomes constant, whereas CERC has no dependence,
– increases with beach slope (for slopes>0.01), whereas CERC has no dependence,
– first decreases, then increases with grain-size.

Overall, the new formula (for $A_4=1.0$) gives results smaller than the CERC formula by a factor of between 12 and 40. This is consistent with observations that the CERC formula greatly over-estimates transport of

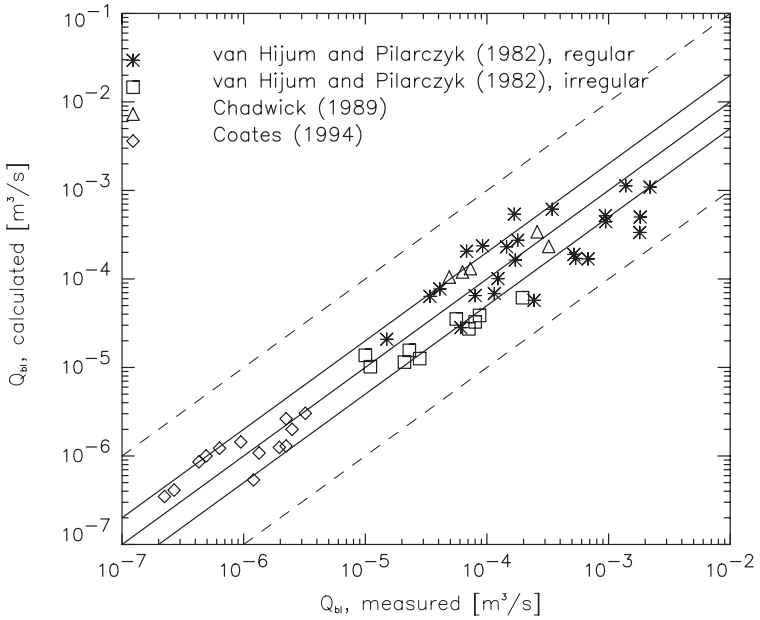

Fig. 7. Comparison of Eqs. (51)–(55) with data, for $A_4=1.0$.

Table 1
Percentage of predictions lying within factors 2, 5 and 10 of measured values

	Factor 2	Factor 5	Factor 10
Current alone (coefficient=8)	91	100	100
Current alone (coefficient=12)	91	100	100
Asymmetric waves alone	62	87	87
Waves and currents	47	85	98
Longshore transport	60	98	100

shingle (a reduction factor of 18 is commonly introduced when using the CERC formula for shingle). The factor of 40 applies to 0.2 mm sand, and includes the fact that the CERC formula is a total load formula, whereas the new formula only applies to bedload transport. The increase of transport with grain-size (for cases well above threshold) seems contrary to expectations, but is consistent with the many well-accepted bedload formulae that have a dependence on $\theta^{3/2}$ (e.g. Meyer-Peter and Müller, 1948). The increase occurs because the current drag coefficient and the wave friction factor increase with grainsize.

The calibrated formulae have been applied to a number of shingle field and laboratory data sets: Van Hijum and Pilarczyk (1982) did laboratory experiments at Delft Hydraulics with shingle transport under the action of regular and irregular waves. Chadwick (1989) collected field data of longshore shingle transport near Brighton, UK, and Coates (1994) did physical model studies of shingle transport at HR Wallingford. The results are shown in Fig. 7. Most transport rates are predicted within a factor 2 and all data sets are predicted within a factor 10.

6. Conclusions

We have developed a number of analytical formulae for bedload sediment transport rates that are of use in practical coastal applications, especially for gravel-sized materials. These apply to:

a) Steady currents in rivers, or tidal and wind-driven currents in the sea, given by Eq. (13),
b) Current plus symmetrical (sinusoidal) waves at an arbitrary angle, given by Eqs. (23)–(28),
c) Current plus asymmetrical waves at an arbitrary angle, given by Eqs. (31)–(35),
d) Asymmetrical waves alone, producing net bedload transport due to crest-trough asymmetry, given by Eq. (36),
e) Integrated longshore transport produced by waves incident at an angle to a plane, linear beach, given by Eqs. (51)–(55).

The coefficient A_2 appearing in these formulae takes values between 8 and 12, depending on the shape, angularity and degree of sorting of the sediment grains. Where possible, the coefficient should be determined by fitting to specific sediments. If this is not possible, set $A_2=10$ as a default value, with an uncertainty of $\pm 20\%$. The value of A_4 in Eqs. (51)–(55) was calibrated against field measurements on a shingle beach as $A_4=1.0$.

The formulae were tested against measurements where possible, and the percentage of predictions lying within factors of 2, 5 and 10 were calculated. These are summarised in Table 1. The percentage lying within a factor of 2 is greatest for the simplest case of currents alone (91%, for both $A_2=8$ and 12) and decreases to 47% for the most complex case of combined waves and currents. The longshore transport predictor gives good agreement with laboratory and field data over four orders of magnitude, with 60% lying within a factor of 2 of the data.

Acknowledgements

Part of this work was funded by the EC collaborative research project SEDMOC (MAST Project No MAS3-C797-0115). The authors are grateful to Dr. JFA Sleath for providing access to his data, and to Ms. Lisa Hall for her careful programming and plotting.

References

Al-Salem, A.A. (1993). Sediment transport in oscillatory boundary layer under sheet flow conditions. PhD thesis, Technical University of Delft, The Netherlands.

CERC, 1984. Shore protection manual, vols I to III. US Army Corps of Engineers, Coastal Engineering Research Centre, US Govt Printing Office.

Chadwick, A.J., 1989. Measurements and numerical model verification of coastal shingle transport. In: Palmer, M.H. (Ed.), Advances in Water Modelling and Measurement. British Hydromechanics Research Association, Cranfield, UK.

Coates, T.T. (1994). Effectiveness of control structures on shingle beaches. HR Wallingford Report SR387.

Damgaard, J.S., Soulsby, R.L., 1997. Longshore bed-load transport. Proc. 25th International Conference on Coastal Engineering. Orlando, Florida, USA, pp. 3614–3627.

Damgaard, J.S., Stripling, S., Soulsby, R.L., 1996. Numerical Modelling of Coastal Shingle Transport. Report TR4. HR Wallingford Ltd., Wallingford, UK.

Damgaard, J.S., Whitehouse, R.J.S., Soulsby, R.L., 1997. Bed-load sediment transport on steep longitudinal slopes. J. Hydraul. Eng. 123 (12), 1130–1138.

Engelund, F., Fredsøe, J., 1976. A sediment transport model for straight alluvial channels. Nord. Hydrol. 7, 293–306.

Fredsøe, J., Deigaard, R., 1992. Mechanics of Coastal Sediment Transport. Advanced Series on Ocean Engineering, vol. 3. World Scientific, Singapore.

Grant, W.D., Madsen, O.S., 1979. Combined wave and current interaction with a rough bottom. J. Geophys. Res. 84 (C4), 1797–1808.

Kaczmarek, L.M., 1999. Moveable Sea Bed Boundary Layer and Mechanics of Sediment Transport. Institute of Hydroengineering of the Polish Academy of Sciences (IBW PAN), Poland.

King, D.B. (1991). Studies in oscillatory flow bed-load sediment transport. PhD thesis, University of California, San Diego, USA.

Lee-Young, J.S. (1988). Bed mechanics in combined steady and oscillatory flow. PhD thesis, University of Cambridge, UK.

Lodahl, C.R., Sumer, B.M., Fredsøe, J., 1998. Turbulent combined oscillatory flow and current in a pipe. J. Fluid Mech. 373, 313–348.

Madsen, O.S., 1991. Mechanics of Cohesionless Sediment Transport in Coastal Waters. Proc. Coastal Sediments. '91, ASCE, New York, USA, pp. 15–27.

Meyer-Peter, E., Müller, R., 1948. Formulas for bed-load transport. Rep. 2nd Meeting Int. Assoc. Hydraul. Struct. Res., Stockholm, Sweden, pp. 39–64.

Myrhaug, D., Holmedal, L.E., Rue, H., in press. Bottom friction and bedload transport caused by boundary layer streaming beneath random waves, Appl. Ocean Res.

Nielsen, P., 1992. Coastal bottom boundary layers and sediment transport. Advanced Series on Ocean Engineering, vol. 4. World Scientific Publishing, Singapore.

Pugh, F.J., Wilson, K.C., 1999. Velocity and concentration distributions in sheet flow above plane beds. Proc. ASCE, J. Hydraul. Eng. 125 (2), 117–125.

Simons, R.R., Grass, A.J., Mansour-Tehrani, M., 1993. Bottom shear stresses in the boundary layers under waves and currents crossing at right angles. Proc. 23rd International Conference on Coastal Engineering. Venice, Italy, pp. 604–617.

Simons, R.R., Myrhaug, D., Thais, L., Chapalain, G., Holmedal, L.E., MacIver, R., 2001. Bed friction in combined wave-current flows. Proc. 27th International Conference on Coastal Engineering. Sydney, Australia, pp. 216–226.

Sleath, J.F.A., 1978. Measurements of bed load in oscillatory flows. Proc. ASCE, J. Waterw., Port, Coastal., Ocean Eng. Div. 104 (WW3), 291–307.

Sleath, J.F.A., 1994. Sediment transport in oscillatory flow. In: Belorgey, M., Rajaona, R.D., Sleath, J.F.A. (Eds.), Sediment Transport Mechanisms in Coastal Environments and Rivers. World Scientific Publishing, Singapore.

Sleath, J.F.A., 1995. Sediment transport by waves and currents. J. Geophys. Res. 100 (C6), 10977–10986.

Soulsby, R.L., 1997. Dynamics of Marine Sands. A Manual for Practical Applications. Thomas Telford, London, UK.

Soulsby, R.L., Clarke, S., 2004. Bed Shear-Stresses Under Combined Waves and Currents on Smooth and Rough Beds. Report TR 137. HR Wallingford Ltd., Wallingford, UK.

Soulsby, R.L., Damgaard, J.S., 2005. Bedload Sediment Transport in Coastal Waters. Report TR152. HR Wallingford Ltd., Wallingford, UK.

Sumer, B.M., Kozkiewicz, A., Fredsoe, J., Deigaard, R., 1996. Velocity and concentration profiles in sheet-flow layer of movable bed. ASCE J. Hydraul. Eng. 122 (10), 549–558.

Van Hijum, E., Pilarczyk, K.W., 1982. Equilibrium profile and longshore transport of coarse material under regular and irregular wave attack. Publication No. 274. Delft Hydraulics, Delft, The Netherlands.

Wilson, K.C., 1966. Bed-load transport at high shear stress. Proc. ASCE, J. Hydraul. Div. 92 (HY6), 49–59.

Wilson, K.C., 1989. Friction of wave induced sheet flow. Coast. Eng. 12, 371–379.

Zala Flores, N., Sleath, J.F.A., 1998. Mobile layer in oscillatory sheet flow. J. Geophys. Res. 103 (C6), 12783–12793.